Comparing the Effects of Failures in Power Grids under the AC and DC Power Flow Models

Cetinay, Hale; Soltan, Saleh; Kuipers, Fernando A.; Zussman, Gil; Van Mieghem, Piet

DOI
10.1109/TNSE.2017.2763746

Publication date
2018

Document Version
Accepted author manuscript

Published in
IEEE Transactions on Network Science and Engineering

Citation (APA)
Cetinay, H., Soltan, S., Kuipers, F. A., Zussman, G., & Van Mieghem, P. (2018). Comparing the Effects of Failures in Power Grids under the AC and DC Power Flow Models. *IEEE Transactions on Network Science and Engineering*, *5*(4), 1-12. https://doi.org/10.1109/TNSE.2017.2763746

Comparing the Effects of Failures in Power Grids under the AC and DC Power Flow Models

Hale Cetinay, Saleh Soltan, Fernando A. Kuipers, Gil Zussman, and Piet Van Mieghem

Abstract—In this paper, we compare the effects of failures in power grids under the nonlinear AC and linearized DC power flow models. First, we numerically demonstrate that when there are no failures and the assumptions underlying the DC model are valid, the DC model approximates the AC model well in four considered test networks. Then, to evaluate the validity of the DC approximation upon failures, we numerically compare the effects of single line failures and the evolution of cascades under the AC and DC flow models using different metrics, such as yield (the ratio of the demand supplied at the end of the cascade to the initial demand). We demonstrate that the effects of a single line failure on the distribution of the flows on other lines are similar under the AC and DC models. However, the cascade simulations demonstrate that the assumptions underlying the DC model (e.g., ignoring power losses, reactive power flows, and voltage magnitude variations) can lead to inaccurate and overly optimistic cascade predictions. Particularly, in large networks the DC model tends to overestimate the yield. Hence, using the DC model for cascade prediction may result in a misrepresentation of the gravity of a cascade.

Index Terms—Power grids, AC versus DC, power flows, cascading failures, contingency analysis.

1 Introduction

Power grids are vulnerable to external events, such as natural disasters and cyber-attacks, as well as to internal events, such as unexpected variability in load or generation, aging, and control device malfunction. The operation of a power grid is governed by the laws of physics [1], and the outage of an element may result in a cascade of failures and a blackout [2]. The recent blackouts in Turkey [3], India [4], U.S. and Canada [5] had devastating effects and as such motivated the study of power grid vulnerabilities to cascading failures (e.g., [2], [6], [7], [8]).

Some of the recent work on cascading failures considers a topological perspective where, once a network element fails, the neighboring elements also fail [9]. However, such topological models do not consider the actual power grid flow dynamics. More realistic cascading failures models use the linearized direct current (DC) power flows [10], [11]. However, DC power flows are based on a linearization of the nonlinear AC power flow dynamics. The induced linearization error can be small in large transmission grids [12] and high for some particular networks [13]. Motivated by these observations, *we study the effects of line failures and cascades under both the linearized DC model and a nonlinear AC model* by performing simulations on four test networks.

First, we numerically evaluate the accuracy of the DC power flow model when there are no failures. We demonstrate that when there are no failures, the assumptions underlying the DC power flow approximation (i.e., negligible active power losses, reasonably small phase angle differences between the neighboring nodes, and small variations in the voltage magnitudes at nodes) are valid, and therefore, the DC power flow model approximates the AC power flow model relatively well in four considered test networks. We further derive an analytical upper bound on the difference between the AC and the DC power flows based on the accuracy of the DC approximation assumptions. The analytical results appear in the Appendix. These results quantify the accuracy of the DC power flow model based on the accuracy of the approximation assumptions.

Then, we compare the effects of single line failures under the AC and DC models. We numerically demonstrate that the DC model can also capture the effects of a single line failure on the flow changes on other lines relatively close to the AC model. For example, in nearly 80% and 98% of the observed values in the IEEE 30-bus network and Polish grid, respectively, the magnitudes of the differences in the line flow change ratios (the ratio of the change in the flow on a line after a failure to its original flow value) and the line outage distribution factors (the ratio of the change in the flow on a line after a failure to the flow value of the failed line) are smaller than 0.05.

We then present an AC cascading failures model which is based on the nonlinear power flow equations, and therefore, is more realistic than the corresponding DC model. We empirically compare the AC and DC cascade models based on robustness metrics that quantify the operational and topological characteristics of the grid during a cascade for all cascading failures initiated by a single and two line failures. Our simulations demonstrate that the assumptions underlying the DC model (lossless network and ignoring reactive power flows and voltage variations) can lead to inaccurate and overly optimistic cascade predictions. For example, in the Polish grid, the difference between the yield

- *H. Cetinay, F. A. Kuipers, and P. Van Mieghem are with the faculty of Electrical Engineering, Mathematics and Computer Science, Delft University of Technology, Delft, The Netherlands. E-mails: {H.Cetinay-Iyicil, F.A.Kuipers, P.F.A.VanMieghem}@tudelft.nl*
- *S. Soltan is with the Elec. Eng. Dept., Princeton University, Princeton, NJ. This work was done while Saleh Soltan was with Columbia University. E-mail: ssoltan@princeton.edu.*
- *G. Zussman is with the Elec. Eng. Dept., Columbia University, New York, NY. E-mail: gil@ee.columbia.edu.*

(the ratio of the demand supplied at the end of the cascade to the initial demand) under the AC and DC cascade models is more than 0.4, in 60% of the cascades initiated by two line failures.

Moreover, we empirically compare the AC and DC cascades under different supply and demand balancing and line outage rules. Our simulation results show that the difference between the cascade evolution under the AC and DC power flows depends on the balancing and line outage rules in power grids. In particular, the supply and demand balancing rule which separates the excess supply or demand from the grid increases the difference between the AC and DC models the most.

The remainder of this paper is organized as follows. Section 2 reviews related work and Section 3 presents the power flow equations. Section 4 presents the cascading failures models. Section 5 presents the numerical comparison of the AC and DC flow models in four different test networks and Section 6 concludes the paper. Analytical results on the difference between the AC and DC power flow models appear in the Appendix.

2 Related Work

Contingency analysis and cascading failures in power grids have been widely studied [2], [7], [14], [15], [16], [17]. In this section, we briefly review some of the methods and their relation to our work. We note that there are several abstract models, borrowed from physics, for modeling cascades in power grids (e.g., see [9], [18], [19], [20]). These models do not include the power-flow dynamics in power grids and, hence, are out of scope of this paper.

The study of cascading failures in power grids was initiated in [21], [22] which used the linearized DC model and a probabilistic outage rule for overloaded line failures. Similar cascade models have been used to study the properties of the cascades [11], [23], [24], [25], [26], [27], [28], as well as to design control schemes to mitigate the cascade [29], [30] and to detect vulnerable parts of the grid [7], [11], [31].

Due to their complexity, the AC power flow equations are not as commonly used as the DC equations in studying cascading failures in power grids. An AC model is utilized in [7], [32], as well as in some (mostly commercial) software tools for modeling the evolution of the cascade [33]. Unfortunately, none of these tools is publicly available. Hence, for the evaluation in this paper, we developed an AC cascading failures simulator [34], using the MATPOWER AC power flow solver [35].

Previous work on determining the accuracy of the DC power flow approximation includes [12], [13], [36], [37], [38], [39], [40]. However, these works did not consider accuracy of the DC flows in predicting the evolution of a cascade. In [7], the DC and the AC cascading failures are compared when all the buses (nodes) in the AC model are voltage controlled (PV) buses. *To the best of our knowledge, this paper is the first to compare the evolution of cascades in power grids under the DC and AC power flows in detail and for many of the publicly available power grid networks [35], [41].*

3 Power Flow Equations

In this section, we provide details on the AC and DC power flow equations.

3.1 AC Power Flow Equations

A power grid with n nodes (buses) and m transmission lines constitutes a complex network whose underlying topology can be represented by an undirected graph $\mathcal{G}(\mathcal{N}, \mathcal{L})$, where $\mathcal{N}$ denotes the set of nodes and $\mathcal{L}$ denotes the set of lines. Each line l has a predetermined capacity c_l that bounds its flow $|f_l|$ under a normal operation of the system. The status of each node i is represented by its voltage $V_i = |V_i|e^{\mathbf{i}\theta_i}$ in which $|V_i|$ is the voltage magnitude, θ_i is the phase angle at node i, and $\mathbf{i}$ denotes the imaginary unit.

The goal of an AC power flow analysis is the computation of the voltage magnitudes and phase angles at each bus in steady-state conditions [42]. In the steady-state, when the admittance values to ground are negligible, the injected apparent power S_i at node i equals to

$$S_i = \sum_{\substack{k=1 \\ k\neq i}}^{n} S_{ik} = \sum_{\substack{k=1 \\ k\neq i}}^{n} V_i y_{ik}^*(V_i^* - V_k^*) = V_i(\mathbf{YV})_i^* \qquad (1)$$

where * denotes the complex conjugation, $\mathbf{V} = [V_1, \ldots, V_n]^{\mathrm{T}}$ is the vector of node voltages, y_{ik} is the equivalent admittance of the lines from node i to k, and $\mathbf{Y}$ is the $n \times n$ admittance matrix. The elements of the admittance matrix $\mathbf{Y}$, which depend on the topology of the grid as well as the admittance values of the lines, are defined as follows:

$$Y_{ik} = \begin{cases} \sum_{i\neq k} y_{ik}, & \text{if } k = i \\ -y_{ik}, & \text{if } k \in N(i) \\ 0, & \text{if } k \notin N(i) \end{cases}$$

where $N(i)$ denotes the direct neighbors of node i.

Rewriting the admittance matrix as $\mathbf{Y} = \mathbf{G} + \mathbf{iB}$ where $\mathbf{G}$ and $\mathbf{B}$ are real matrices, and using the definition of the apparent power $S_{ik} = P_{ik}^{(\mathrm{AC})} + \mathbf{i}Q_{ik}^{(\mathrm{AC})}$ in (1) leads to the equations for the active power P_i and the reactive power Q_i at each node i:

$$P_i = \sum_{k=1}^{n} |V_i||V_k|(G_{ik}\cos\theta_{ik} + B_{ik}\sin\theta_{ik}) \qquad (2)$$

$$Q_i = \sum_{k=1}^{n} |V_i||V_k|(G_{ik}\sin\theta_{ik} - B_{ik}\cos\theta_{ik}) \qquad (3)$$

where $\theta_{ik} = \theta_i - \theta_k$.

In the AC power flow analysis, each node i is categorized into one of the following three types:

1) *Slack node*: The node for which the voltage is typically 1.0. For convenience, it is indexed as node 1. The slack node compensates for network losses by emitting or absorbing power. The active power P_1 and the reactive power Q_1 need to be computed.
2) *Load node*: The active power P_i and the reactive power Q_i at these nodes are known and the voltage V_i needs to be computed.
3) *Voltage controlled node*: The active power P_i and the voltage magnitude $|V_i|$ at these nodes are known and the reactive power Q_i and the phase angle θ_i need to be computed.

3.2 DC Power Flow Equations

The AC power flow equations are nonlinear in the voltages. The DC power flow equation provides a linearized approximation of the active power flows in the AC model. Linearization is possible under the following conditions [42]:

1) The difference between the voltage phase angles of every couple of neighboring nodes is small such that $\sin\theta_{ik} \approx \theta_{ik}$ and $\cos\theta_{ik} \approx 1$.
2) The active power losses are negligible, and therefore, $\mathbf{Y} \approx \mathbf{iB}$ where $\mathbf{B}$ is the imaginary part of the admittance matrix $\mathbf{Y}$, calculated neglecting the line resistances.
3) The variations in the voltage magnitudes $|V_i|$ are small and, therefore, it is assumed that $|V_i| = 1\ \forall i$.

Under these assumptions, given the active power P_i at each node i, the phase angle of the nodes can be estimated by $\tilde{\theta}_i$ using the DC power flow equations as follows:

$$P_i = \sum_{\substack{k=1 \\ k\neq i}}^{n} P_{ik}^{(\mathrm{DC})} = \sum_{\substack{k=1 \\ k\neq i}}^{n} B_{ik}(\tilde{\theta}_i - \tilde{\theta}_k) \tag{4}$$

or in matrix form,

$$\tilde{\mathbf{P}} = -\mathbf{B}\tilde{\mathbf{\Theta}} \tag{5}$$

where $\tilde{\mathbf{P}} = [\tilde{P}_1, P_2, \ldots, P_n]^{\mathrm{T}}$, $\tilde{\mathbf{\Theta}} = [\tilde{\theta}_1, \ldots, \tilde{\theta}_n]^{\mathrm{T}}$. Notice that the vectors $\mathbf{P}$ and $\tilde{\mathbf{P}}$ are equal except in the *slack node* (first entry) since in the DC power flows, the lines are lossless and therefore $\tilde{P}_1 + \sum_{i=2}^{n} P_i = 0$.

By assuming that the phase angle at the slack node is 0, the phase angle of the nodes can be estimated uniquely by solving (5) for the DC power flow.

In Section 5, we numerically compare the AC and DC power flow models and demonstrate that when there are no failures, the DC power flows provide relatively accurate approximation of the AC power flows on most of the network lines. For more details of the DC power flow model and its analytical accuracy based on the three assumptions, see the Appendix.

4 Modeling Cascading Failures

An initial failure in power grids may result in subsequent failures in other parts of the grid. These consecutive failures following an initial failure constitute a *cascading failure*. In this section, we follow [7], [10], [14], [28] and develop models for cascading failures due to line failures in power grids.

Before a cascading failure, we assume that $\mathcal{G}(\mathcal{N}, \mathcal{L})$ is connected, the power flows satisfy (2) and (3) or (5), and the flow magnitude $|f_l|$ of each line is at most its capacity c_l.

Next, we describe the cascading failures models. When an initial set of lines fail, they are removed from the network. As a result of this removal, the network topology is changed, and the power grid can be divided into one or more connected components. Following [10], we assume that each connected component can operate autonomously. If there is no supply or no demand within a connected component $\mathcal{G}_k$, the component becomes a *dead component*, and all the demand or supply nodes within the component are put out of service. If there are both supply and demand nodes within a connected component $\mathcal{G}_k$, the connected component remains an *alive component*, but the supply and demand within the component should be balanced. We use two different supply and demand balancing rules [7], [10], [14]:

1) *Shedding and curtailing:* The amount of the power supply or demand are reduced at all nodes by a common factor. If the total active power supply is more than the total active power demand in a connected component $\mathcal{G}_k$, the active power outputs of generators are curtailed. On the other hand, if the total active power supply is not sufficient to serve the total active power demand, load shedding is performed to balance the supply and demand within $\mathcal{G}_k$.
2) *Separating and adjusting:* Excess supply or demand nodes are separated from the grid. In this case, we assume that the dynamic responses of the generators (demand nodes) are related to their sizes [1]. Namely, the generators (demand nodes) with lower amounts of power output are assumed to be faster to respond to the imbalances between supply and demand. Thus, within each component $\mathcal{G}_k$ with excess supply (demand), the generators (demand nodes) are separated from the grid according their sizes from the smallest to largest until the removal of one more generator (demand node) results in the shortage of supply (demand). Then, the active power output (demand) of the largest supply (demand) node is reduced in order to balance supply and demand.

After supply and demand are balanced within each alive component using the selected balancing rule, the power flow equations are solved to compute new flows on the lines. Note that the line capacities are not taken into account in determining the flows. The new set of line failures are then found in all alive components. We use two different line outage rules [7], [14], [28]:

1) *Deterministic:* A line l fails when the power flow magnitude on that line, denoted by $|f_l|$, exceeds its capacity c_l.
2) *Probabilistic:* A line l fails with probability p_l at each stage of the cascade. We assume that each line l with a flow capacity c_l has also a nominal power flow level $\xi_l \in [0, c_l]$, after which the line may fail with a certain probability (due to increase in line temperature or sag levels). Under this model, the probability p_l is approximated as:

$$p_l = \begin{cases} 0, & \text{if } |f_l| < \xi_l \\ \frac{|f_l| - \xi_l}{c_l - \xi_l}, & \text{if } \xi_l \leq |f_l| < c_l \\ 1, & \text{if } |f_l| \geq c_l. \end{cases} \tag{6}$$

After finding the new set of line failures using the selected line outage rule, the cascade continues with the removal of those lines. If there are no new line failures in any of the alive components, the cascade ends.

In this paper, we study three cascade processes:

I) Cascade with shedding and curtailing balancing rule and deterministic line outage rule,
II) Cascade with separating and adjusting balancing rule and deterministic line outage rule,
III) Cascade with shedding and curtailing balancing rule and probabilistic line outage rule.

In order to study the differences between the AC and DC models, we mostly focus on the cascade process I with shedding and curtailing balancing rule and deterministic line outage rule. In order to further capture the effects of these processes on the differences obtained under the AC and DC models, in Subsection 5.5, we briefly compare the three cascade processes.

In the following two Subsections, we provide the details of the cascade models under the AC and DC power flows.

4.1 AC Cascading Failures Model

In the cascade under the AC power flow model, the flows are composed of active parts P_i in (2) and reactive parts Q_i in (3). Hence, the apparent power S_i in (1) is used to calculate the flows. In general, due to transmission line impedances, the voltage at the sending node of a line is different than the one at the receiving node, resulting in different values of the apparent power flows at each side of the line. Hence, in the cascade under the AC model, we define the magnitude $|f_l|$ of flow on a line $l = \{i, k\}$ as follows:

$$|f_l| = \frac{|S_{ik}| + |S_{ki}|}{2}. \tag{7}$$

The difference, $S_{ik} - S_{ki}$, between the sent and received apparent flows on a line l represents the power loss over that line. The sum of the losses over all the lines is the total loss in the network. The total loss cannot be calculated in advance and is only known after the power flow equations in (1) are solved. Therefore, in the cascade under the AC flow, a part of the total supply in the network is reserved to supply the network losses and denoted by the *reserved loss factor* η.

The case of zero reserved loss factor, $\eta = 0$, means that no reserve supply is allocated for network losses, whereas a large reserved loss factor η corresponds to a large reserve supply for the network losses. Once the power flow equations are solved and the network losses are calculated, the difference between the allocated supply and the total demand with losses is compensated by the slack-node. Therefore, in the AC cascading failures model, the simulation is slack-node dependent, and for every alive component without such a node, a slack-node must be assigned. The developed model chooses the slack-node as the voltage controlled node with the maximum power output in that alive component.

The iterative process of solving the AC power flow equations (2) and (3) may result in the absence of a solution or a divergence in iterations. In such cases, it is perceived that the connected component cannot function at those operational conditions, and supply and demand shedding is applied. The amount of active and reactive power demands, and active power supply within that component are decreased until either convergence is reached in the flow equations or the component becomes a dead component with no demand.

We numerically study the three cascade processes under the AC power flow model in Section 5.

4.2 DC Cascading Failures Model

In the cascade under the DC power flow model, the magnitude $|f_l|$ of the flow on a line $l = \{i, k\}$ is equal to the magnitude of active power flow in (4) on that line:

$$|f_l| = |P_{ik}| = |P_{ki}|. \tag{8}$$

Since the network is assumed to be lossless, the magnitude of the active power at the sending side of a line is equal to the magnitude of active power at the receiving side, $|P_{ik}| = |P_{ki}|$, and the total supply is equal to the total demand. Therefore, the supply and demand balancing is performed without a reserved loss factor η. Moreover, the no-loss assumption means that the flows in the network are slack-node independent.

Contrary to the AC power flow equations (2) and (3), which are nonlinear, the DC power flow equations (5) are linear, and a solution always exists for a connected network with balanced supply and demand [43]. Hence, no supply or demand shedding due to convergence issues is needed in the DC model.

We numerically study the three cascade processes under the DC power flow model in Section 5.

5 Numerical Comparison of the AC and DC Flow Models

This section presents the numerical comparison of the AC and DC power flow models. After providing the simulations setup, we numerically evaluate the accuracy of the DC power flow model when there are no failures. Then, we compare the effects of single line failures, and the evolution of the cascade process I initiated by single and two line failures under the AC and DC flow models. Next, we compare the three cascade processes under the AC and DC flow models. Finally, we discuss the main lessons learned from the simulations.

5.1 Simulations Setup

5.1.1 Metrics

We define metrics for evaluating the grid vulnerability (some of which were originally used in [11], [28], [43], [44]). To study the effects of a *single line e failure* on the flows on other lines we define:

► **Line flow change ratio ($s_{l,e}$)**: the ratio $\Delta f_l / f_l$ of the change Δf_l in the flow on a line l due to the failure at line e to its original flow value f_l.

► **Line outage distribution factor ($m_{l,e}$)**: the ratio $\Delta f_l / f_e$ of the change Δf_l in the flow on a line l due to the failure at line e to the flow value f_e of the failed line e.

Additionally, we define the following metrics to measure other dynamics of the system after a single line failure, which can only be captured under the AC power flow model due to the DC power flow assumptions 2 and 3 in Section 3.2:

► **Node voltage change ($\Delta v_{i,e}$)**: the change in the voltage magnitude at node i after the failure at line e.
► **Power loss change ratio ($\Delta p_{\mu,e}$)**: the ratio of the change in the active power output of the slack generator due to the failure at line e to the initial loss.

We also define metrics to evaluate the *cascade severity*:
► **Node-loss ratio ($N_{\mathcal{G}}$)**: the ratio of the total number of failed nodes (i.e., nodes in dead components) at the end of the cascade to the total number of nodes.
► **Line-loss ratio ($L_{\mathcal{G}}$)**: the ratio of the total number of failed lines at the end of the cascade to the total number of lines.
► **Yield ($Y_{\mathcal{G}}$)**: the ratio of the demand supplied at the end of the cascade to the initial demand.

In addition to the previous metrics which capture the overall effect of a cascading failure on a power grid, we identify the frequently overloaded lines that may cause cascading failures to persist. Hence, we define
► **Line-vulnerability ratio (R_l)**: the total number of cascading failures in which line l is overloaded over the total number of cascading failures simulations. Higher values of R_l indicate the vulnerability of the line l as a possible bottleneck in the network.

5.1.2 Properties of the Networks used in Simulations

We considered four realistic networks: the IEEE 30-bus, the IEEE 118-bus, and the IEEE 300-bus test systems [41], as well as the Polish transmission grid [35]. The details of these networks are as follows.
► **The IEEE 30-bus test system** contains 30 nodes and 41 lines with a total power demand of 189.2 MW.
► **The IEEE 118-bus test system** contains 118 nodes and 186 lines with a total power demand of 4242 MW.
► **The IEEE 300-bus test system** contains 300 nodes and 411 lines with a total power demand of 23,525.85 MW.
► **The Polish transmission grid**, at summer 2008 morning peak, contains 3120 nodes and 3693 lines with a total power demand of 21,181.5 MW.

In the IEEE test networks, maximum line flow capacities are not present. Following [10], the line flow capacities are estimated as $c_l = (1+\alpha)\max\{|f_l|, \overline{f}\}$, where $\alpha = 1$ is the line tolerance, and $\overline{f}$ is the mean of the initial magnitude of line flows.

In the Polish transmission grid data, emergency ratings are used for the flow capacities of the network. In order to eliminate existing overloaded transmission lines at the base case operation, the line flow capacities of such overloaded lines are changed to $c_l = (1+\alpha)|f_l|$ where $\alpha = 1$.

5.1.3 Power Flow Solver

In the simulations, we used MATPOWER [35] package in MATLAB for solving the AC and DC power flows.

5.2 No Failures Case

In this section, we numerically evaluate the accuracy of the DC power flow model when there are no failures in four test networks. First, we check the validity of the assumptions underlying the DC power flow approximation (as mentioned in Section 3.2). Then, we compute the absolute difference between the AC and DC power flow models.

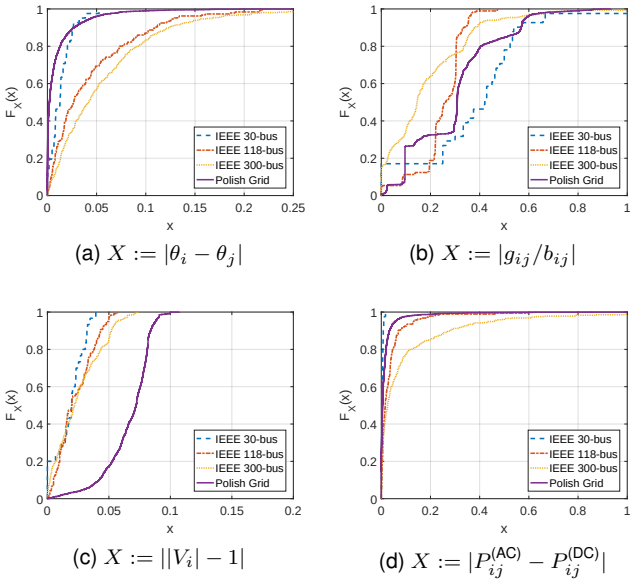

Fig. 1. The validity of the assumptions underlying the DC power flow approximation and the resulting difference between the AC and DC power flow models: the CDFs of (a) the absolute difference between the voltage phase angle of neighboring nodes, (b) the ratio of the real to imaginary part of the admittance values, (c) the deviation of the voltage magnitudes from 1, and (d) the absolute difference of the AC and DC active power flows.

Fig. 1 shows the cumulative distribution functions (CDFs) of the absolute difference between the voltage phase angle of neighboring nodes, the ratio of the real to imaginary part of the admittance values, the deviation of the voltage magnitudes from 1, and the absolute difference of the AC and DC active power flow.

In particular, Fig. 1a demonstrates that the difference between the voltage phase angles of neighboring nodes (condition 1) is less than 0.1 for 80% of the pairs in all test networks. Fig. 1b shows that the imaginary part of the admittance values are dominant (condition 2) in the test networks. Fig. 1c shows that the voltage magnitudes are close to 1.0 (condition 3) for all the nodes. Hence, as can be seen in Fig. 1d, the differences between the AC and DC power flows is less than 0.2 (p.u.) for nearly 80% of the lines.

Fig. 1 demonstrates that the assumptions underlying the DC power flow approximation are valid, and the DC power flows approximate the AC power flows of most of the network lines relatively well when there are no failures. In the following subsections, we show that upon failures, however, the DC approximation may become inaccurate. Moreover, the small differences between the AC and DC power flows in different cascade stages may lead to drastic differences at the end of the cascade.

5.3 Comparison of the Single Line Failure Effects

Single line failure and its consequent removal is the first stage and the triggering event of possible cascading failures. In this section, we perform empirical studies on single line failures in four realistic networks. Since the line flow change ratios $s_{l,e}$ for the lines with a low initial flow can be unreasonably high [11], these values are calculated only for

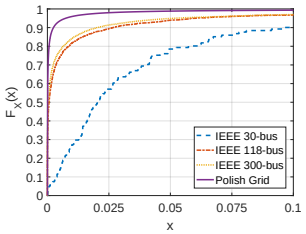

(a) $X := |s^{AC}_{l,e} - s^{DC}_{l,e}|$

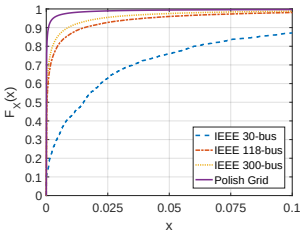

(b) $X := |m^{AC}_{l,e} - m^{DC}_{l,e}|$

Fig. 2. The CDFs of the differences in the line flow change ratios and the line outage distribution factors based on the AC and DC flow models.

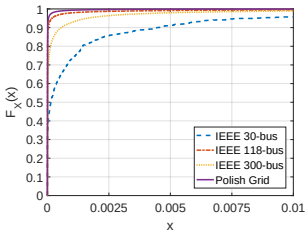

(a) $X := |\Delta v^{AC}_{i,e}|$

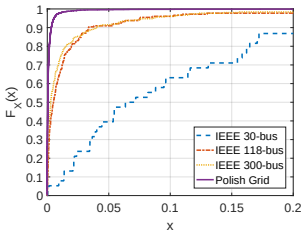

(b) $X := |\Delta p^{AC}_{\mu,e}|$

Fig. 3. The CDFs of the magnitudes of node voltage changes and the power loss change ratios after a single line failure for all the test networks under the AC flow model.

the lines whose initial flow is larger than the mean flow. Additionally, to capture the variations of the line outage distribution factors $m_{l,e}$ and power loss change ratios $\Delta p_{\mu,e}$, line failures that partition the network are not considered in the set of failed lines.

Fig. 2 presents the CDFs of the differences in the line flow change ratios and line outage distribution factors calculated based on the AC and DC flows. These results show that the differences decrease with the size of the network. In nearly 80% of the observed values in the IEEE 30-bus network, the magnitudes of the differences in the line flow change ratios $s_{l,e}$ and the line outage distribution factors $m_{l,e}$ are smaller than 0.05, whereas, in the Polish transmission grid this percentage is nearly 98%.

Since the DC power flow model cannot capture the node voltage changes $\Delta v_{i,e}$ (the node voltages are always equal to 1 under the DC model) and the power loss change ratios $\Delta p_{\mu,e}$ (the network is assumed to be lossless under the DC model) after a line failure, the CDFs of these two metrics are shown in Fig. 3 only for the AC flow model. Fig. 3a shows the absolute changes in the magnitude of the node voltages due to a line failure using the AC model. Both increase and decrease in the values of the node voltages are observed. However, the probability of a decrease is higher as the system continues to operate with fewer lines.

Fig. 3b illustrates the power loss change ratios after a line failure using the AC model. A line failure can lead to an increase or a decrease in the slack node power output. However, the probability of a decrease is quite low since the system's loss generally increases when lines are removed from the grid.

Similar to our observations in Fig. 2, the node voltage changes and power loss ratios generally become smaller with the size n of the network. For the Polish transmission grid, the obtained values of nearly all the node voltage changes and power loss change ratios are smaller than 0.005 and 0.05, respectively.

5.4 Comparison of the Cascade Process I Evolution under the AC and DC Models

The models introduced in Sections 4.1 and 4.2 are used to simulate cascading failures under the AC and DC flow models, respectively. For a fair comparison between the AC and DC models, the loss factor in the AC cascading failures model (in Section 4.1) is taken to be zero. Moreover, the cascade process I is used in this subsection in order to focus on the differences between the AC and DC models.

5.4.1 *Cascading Failures Initiated by a Single Line Failure*

An example of a cascade initiated by a single line failure in the IEEE 118-bus network under the two cascade models is shown in Fig. 4. The basic observation from this figure is that the evolution of the cascade under the two models can be quite different. For instance, in Fig. 4a, there are two overloaded lines at the first stage of the cascade under the AC model which are not overloaded under the DC model. This initial difference results in a considerable difference in the evolution of the cascade: An important flow path in the AC model is failed at the first stage, resulting in more severe consecutive stages. Therefore, the differences between the AC and DC models accumulate at each cascade stage and may lead to *a drastic difference at the end of the cascade*.

To further investigate the differences, we simulate cascading failures due to all single line failures whose initial flows were larger than the mean of initial flows in the four test networks. Figs. 5, 6, 7, and 8 provide the detailed results obtained under the two cascade models.

Fig. 5 shows the scatter plot of the yield values under the two models for the four test networks. It suggests that the yield values obtained by the DC cascade model are usually higher, specially for large networks. Moreover, Fig. 8a, which presents the CDFs of the differences in yield values for all the test networks, also shows that the differences in the obtained yield values can grow quite high in large networks.

In Fig. 6 and Fig. 8b, however, the line-loss ratios are observed to be close under the two cascade models in all the four networks. The same is true for the node-loss ratios (see Fig. 8c). Despite the similarity of the line-loss and node-loss ratios under the two cascade models, Fig. 7, which presents the line-vulnerability ratios, suggests that as networks become larger, the individual lines that fail frequently under the AC model are very different from their counterparts under the DC model (see Figs. 7c and 7d). Fig. 8d also shows that the differences in the line-vulnerability ratios are close for most of the lines, but the differences may be quite large for roughly 10% of the lines in large networks.

5.4.2 *Cascading Failures Initiated by Two-Line Failures*

We study cascades that are triggered by two-line failures. Two-line combinations of all lines whose initial flows are larger than the mean initial flows are investigated in the IEEE 30- and 118-bus networks, whereas, in the IEEE 300-bus network and the Polish transmission grid, 1000 random

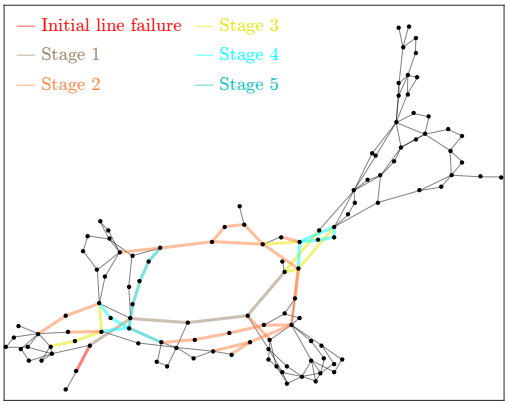

(a) AC cascading failures model

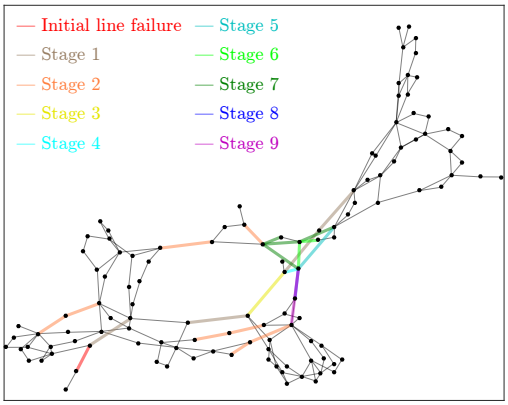

(b) DC cascading failures model

Fig. 4. Evolution of a cascade initiated by a single line failure in the IEEE 118-bus network under the AC and DC cascade models. The remaining load at the end of the simulation is 1594.5 MW under AC cascading failures model, and 2446.3 MW under DC cascading failures model.

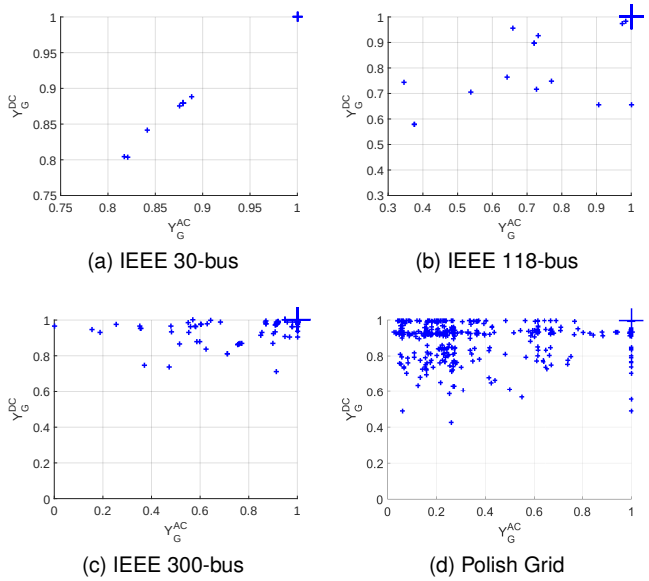

Fig. 5. The scatter plots of the yield values under the AC versus DC cascade models initiated by single line failures. Markers are scaled according to the frequencies of corresponding data points.

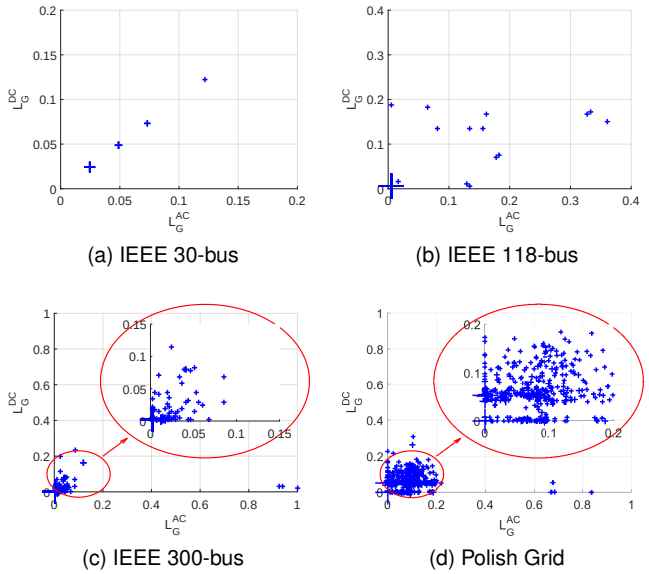

Fig. 6. The scatter plots of the line-loss ratios under the AC versus DC cascade models initiated by single line failures. Markers are scaled according to the frequencies of corresponding data points.

two-line removals are selected out of those combinations. The same set of results as in the previous section are presented in Figs. 9, 10, 11, and 12. Similar observations as in the previous section can be made from these figures for the differences in the cascades initiated by two line failures under the AC and DC cascade models.

Fig. 9 shows the scatter plot of the yield values under the AC and DC cascading failures models for the four test networks. Yield values obtained by the DC cascade model are usually higher, specially for large networks. Fig. 12a presents the CDFs of the differences in yield values for all the test networks. Removal of two lines usually puts the system in a more critical condition with more cascade stages: The magnitudes of the differences in the obtained yield values are slightly higher for the cascades initiated by two line failures than by one line failure.

Fig. 10 and Fig. 12b show the line-loss ratios are still close under the two cascade models in all the four networks. The same is true for the node-loss ratios (see Fig. 12c). However, similar to the yield, the differences in the line-loss and node-loss ratios are slightly higher for the cascades initiated by two line failures than by a single line failure.

Similar to the cascades initiated by single line failures, the lines that fail frequently under the AC model are also different here from their counterparts under the DC model (see Figs. 11c and 11d) when the networks become larger. Fig. 12d also suggests that the differences in the line-vulnerability ratios are also slightly higher here than in the cascades initiated by single line failures.

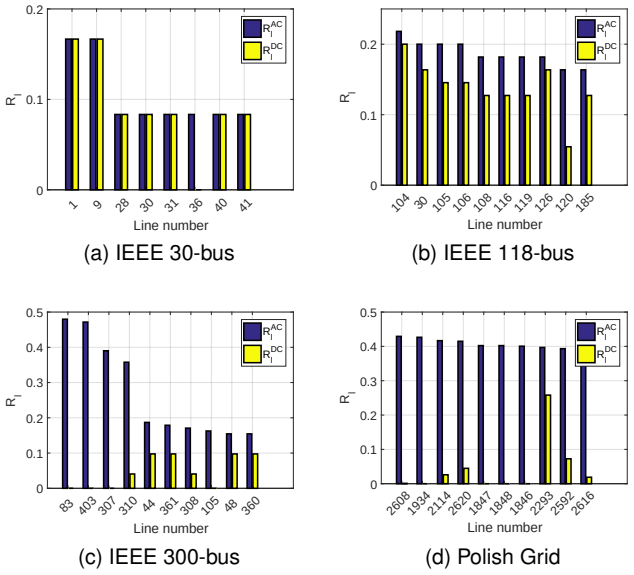

Fig. 7. Comparison between the line-vulnerability ratios under the AC and DC cascade models initiated by single line failures. The lines with the highest line-vulnerability ratios under the AC cascade model are selected for comparison.

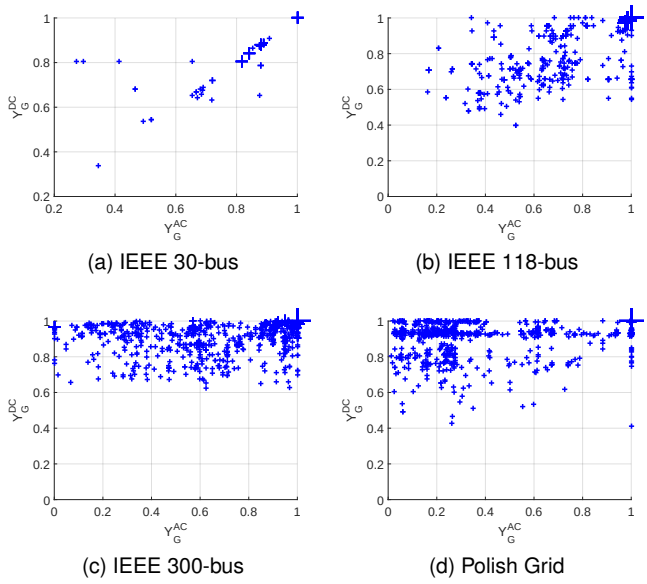

Fig. 9. The scatter plots of the yield values under the AC versus DC cascade models initiated by two-line failures. Markers are scaled according to the frequencies of corresponding data points.

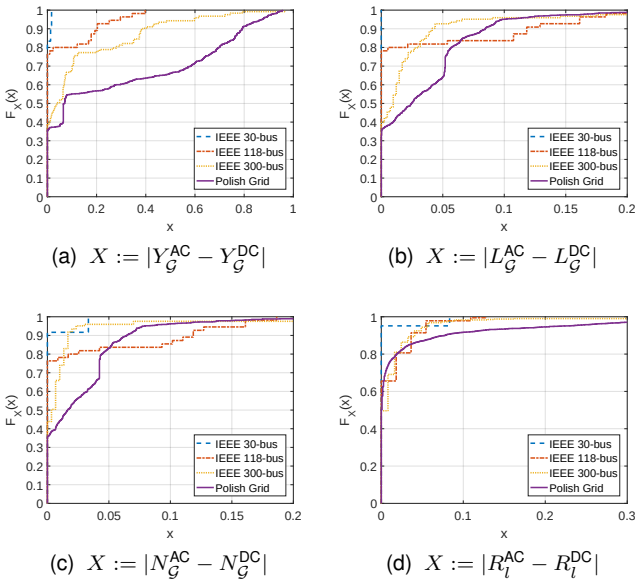

Fig. 8. The CDFs of the differences between the metrics after cascading failures initiated by single line failures under the AC and DC flow models for all the test networks.

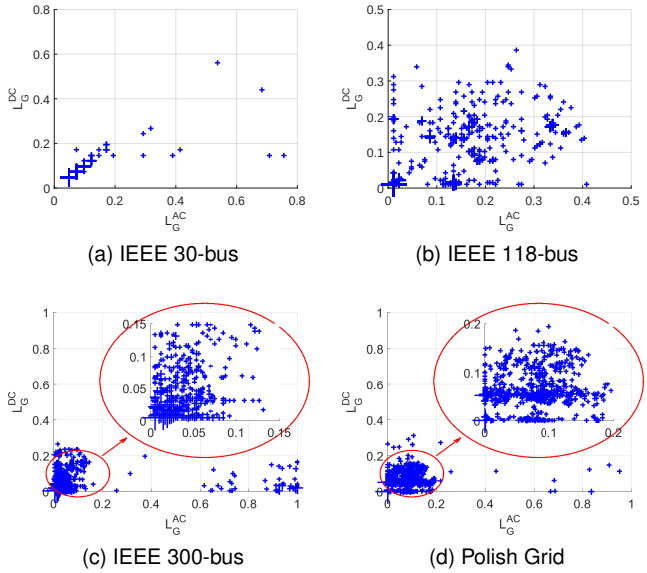

Fig. 10. The scatter plots of the line-loss ratios under the AC versus DC cascade models initiated by two-line failures. Markers are scaled according to the frequencies of corresponding data points.

5.5 Comparison Between the Three Cascade processes under the AC and DC Models

In this subsection, we compare the three cascade processes defined in Section 4 initiated by single line failures under the AC and DC models. For the cascade process III, we set the threshold ξ_l of a line l in (6) as $\xi_l = 0.8 \times c_l$.

Figs. 13-17 provide detailed comparisons between the results obtained under the AC and DC cascade models for the three cascade processes. Fig. 13a and Fig. 13b show the scatter plots of the yield values for cascades in the IEEE 118-bus network and Polish grid. They suggest that the yield values obtained by the cascade process II are generally lower than the other two cascade processes under the AC model. Fig. 17a and Fig. 17b, which present the CDFs of the differences in yield values under the AC and DC cascade models for the three cascade processes in the IEEE 118-bus network and Polish grid, also show that the differences in the obtained yield values under the AC and DC models can grow high for the cascade process II.

Fig. 14a and Fig. 14b show the scatter plots of the line-loss ratios under the AC and DC cascade models for the three cascade processes in the IEEE 118-bus network and Polish grid. Line-loss ratios obtained by the cascade process

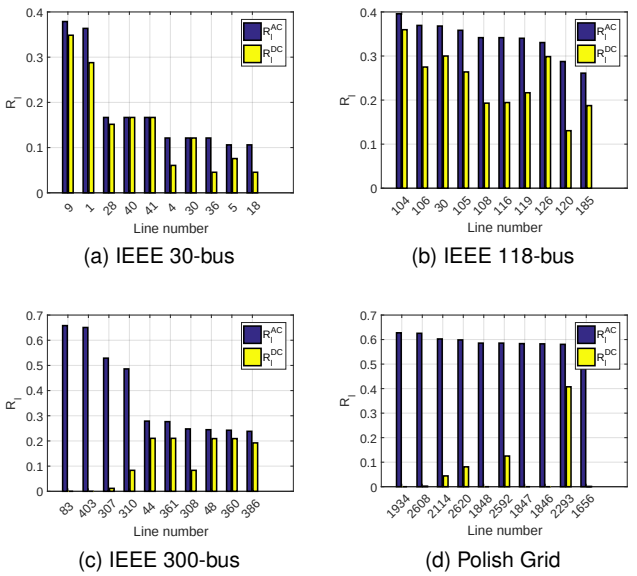

(a) IEEE 30-bus (b) IEEE 118-bus

(c) IEEE 300-bus (d) Polish Grid

Fig. 11. Comparison between the line-vulnerability ratios under AC and DC cascade models initiated by two-line failures. The lines with the highest line-vulnerability ratios under the AC cascade model are selected for comparison.

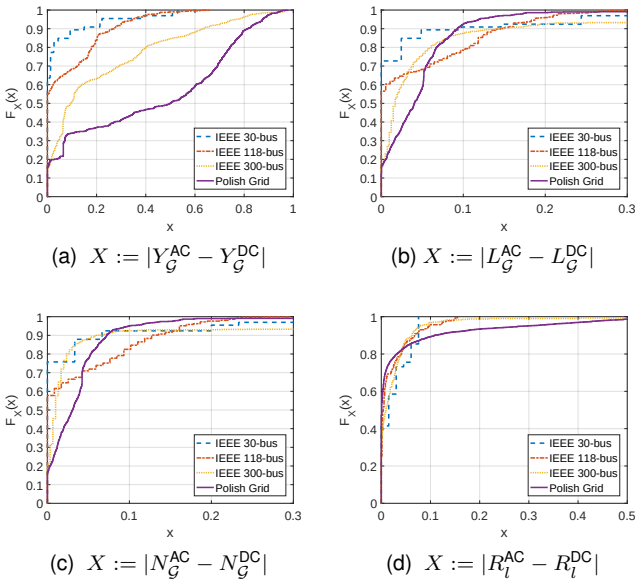

(a) $X := |Y_{\mathcal{G}}^{AC} - Y_{\mathcal{G}}^{DC}|$ (b) $X := |L_{\mathcal{G}}^{AC} - L_{\mathcal{G}}^{DC}|$

(c) $X := |N_{\mathcal{G}}^{AC} - N_{\mathcal{G}}^{DC}|$ (d) $X := |R_l^{AC} - R_l^{DC}|$

Fig. 12. The CDFs of the differences between the metrics after cascading failures initiated by two-line failures under the AC and DC flow models for all the test networks.

II are usually higher, leading to higher differences between the line-loss ratios obtained by the AC and DC flow models. Fig. 17c and Fig. 17d present the CDFs of the differences in line-loss ratios in the IEEE 118-bus network and Polish grid. Similar to Fig. 17a and Fig. 17b, the magnitudes of the differences in the obtained line-loss ratios under the AC and DC models are highest for the cascade process II.

Fig. 15a and Fig. 15b present the comparison between the highest line-vulnerability ratios under the AC and DC cascade models for the cascade process II in the IEEE 118-bus network and Polish grid. Fig. 16a and Fig. 16b present

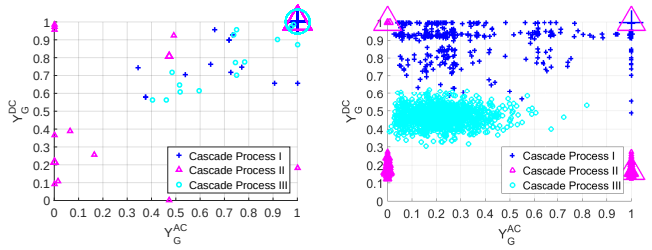

(a) IEEE 118-bus (b) Polish Grid

Fig. 13. The scatter plots of the yield values under the AC vs DC cascade models for the three cascade processes initiated by single line failures. Markers are scaled according to the frequencies of corresponding data points.

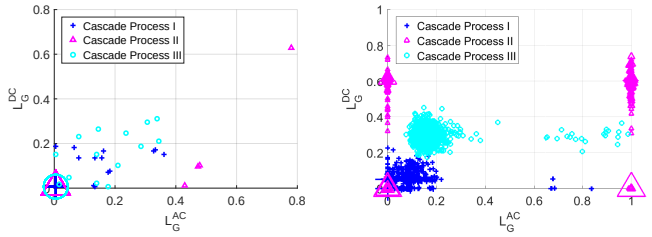

(a) IEEE 118-bus (b) Polish Grid

Fig. 14. The scatter plots of the line-loss ratios under the AC vs DC cascade models for the three cascade processes initiated by single line failures. Markers are scaled according to the frequencies of corresponding data points.

the comparison between the highest line-vulnerability ratios under the the AC and DC cascade models for the cascade process III in the IEEE 118-bus network and Polish grid. The difference between the individual line-vulnerability ratios in Fig. 16b is particularly high for the cascade process III. Fig. 17e and Fig. 17f show that the differences in the line-vulnerability ratios may be quite large for the cascade process III.

Figs. 13-17 suggest that different rules for the supply and demand balancing and line outages could have different effect on the evaluation of the cascades under the AC and DC flow models. In particular, the cascade process II increases the differences between the AC and DC models the most. In this model, by disconnecting many small-sized generators distributed in the network, the demands are supplied by few large-sized generators during the cascade stages. Consequently, the remaining network suffers from low voltage magnitudes and overloaded lines, which can lead to divergence in iterations of AC power flow equations. Moreover, the reactive power flows and voltage magnitudes are not modeled by the DC flow model which can lead to higher differences between the cascades under AC and DC flow models.

Although the cascade process III does not affect the yield values and line-loss ratios very much, its effect is more significant in identifying the most vulnerable set of lines. Due to the probabilistic line tripping model in (6), different lines may trip at each cascade stage, which can result in detecting different sets of vulnerable lines under AC and DC flow models.

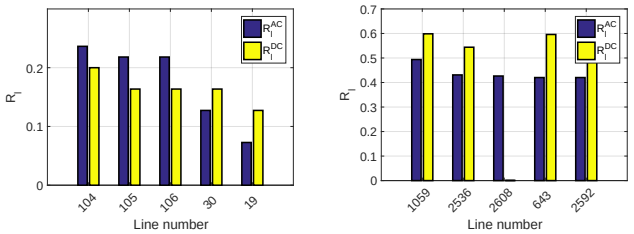

(a) IEEE 118-bus (b) Polish Grid

Fig. 15. Comparison between the line-vulnerability ratios under the AC and DC cascade models for the cascade process II initiated by single line failures. The lines with the highest line-vulnerability ratios under the AC cascade model are selected for comparison.

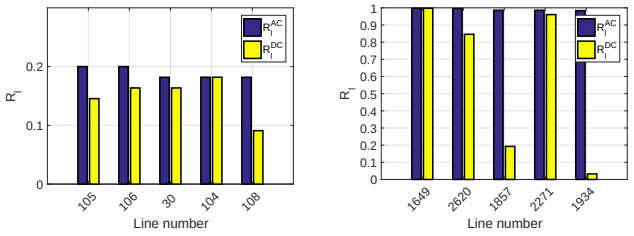

(a) IEEE 118-bus (b) Polish Grid

Fig. 16. Comparison between the line-vulnerability ratios under the AC and DC cascade models for the cascade process III initiated by single line failures. The lines with the highest line-vulnerability ratios under the AC cascade model are selected for comparison.

5.6 Main Lessons Learned from the Simulations

In this section, we summarize the results obtained in the previous subsections. The main lessons learned from the analysis of the DC cascading failures model compared to the AC cascading failures model from the simulations are as follows:

1) When there are no failures and the assumptions underlying the DC power flow approximation are valid, the DC power flow model can approximate the AC power flow model in the network relatively well.
2) The DC power flow model can capture the instant effects of a single line failure on the flow changes on other lines (i.e., line flow change ratios and line outage distribution factors) relatively accurately. However, because of their limitations, they fail to capture other dynamics such as node voltage changes and power loss change ratios.
3) The AC and DC cascade models with the cascade process I provide similar line- and node-loss ratios (i.e., total number of line and node failures) most of the time.
4) The AC and DC cascade models with the cascade process I provide similar yield for small networks. However, for large networks (e.g., the Polish grid) the DC cascade model tends to overestimate the yield.
5) The AC and DC cascade models with the cascade process I agree on the most vulnerable lines under the line-vulnerability ratios in small networks, most of the time. However, for larger networks (i.e., the Polish grid) they tend to detect different sets of lines.
6) The DC cascade model with the cascade process II could underestimate the severity of the cascade compared to AC model with the same cascade process, as the effects of node voltage changes and reactive power flows are neglected under the DC flow model.
7) The AC and DC cascade models with the cascade process III provide similar yield, line-loss, and vulnerability ratios for small networks. However, for larger networks (e.g., the Polish grid) they result in different sets of most vulnerable lines.

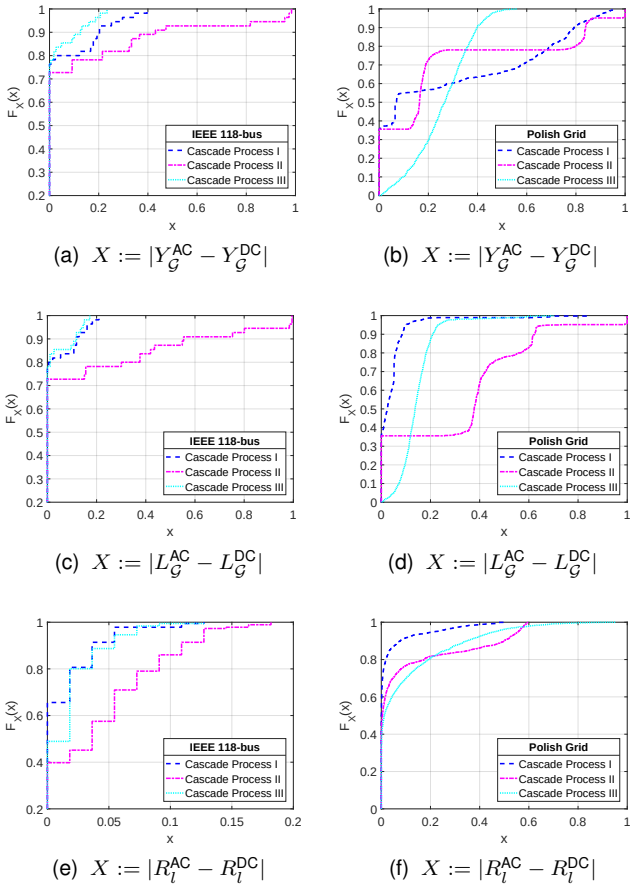

(a) $X := |Y_{\mathcal{G}}^{AC} - Y_{\mathcal{G}}^{DC}|$ (b) $X := |Y_{\mathcal{G}}^{AC} - Y_{\mathcal{G}}^{DC}|$

(c) $X := |L_{\mathcal{G}}^{AC} - L_{\mathcal{G}}^{DC}|$ (d) $X := |L_{\mathcal{G}}^{AC} - L_{\mathcal{G}}^{DC}|$

(e) $X := |R_l^{AC} - R_l^{DC}|$ (f) $X := |R_l^{AC} - R_l^{DC}|$

Fig. 17. The CDFs of the differences between the metrics after cascades under the AC and DC models for the three cascade processes initiated by single line failures in IEEE 118-bus network and Polish grid.

Overall, the obtained results suggest that due to the voltage constraints, the divergence problems, and the reactive power flows, the cascades under the AC flow models are more significant compared to the ones under the DC flow model. Hence, the DC model may underestimate the severity of the cascade, especially for larger networks.

6 Conclusion

In this paper, we thoroughly compared the AC and DC power flow models in describing the state of the grid when there are no failures as well as in predicting the effect of single line failures and the evolution of cascades. We

numerically compared the AC and DC power flow models and demonstrate that when there are no failures, the DC power flow model provides relatively accurate approximation of the AC power flow model. Moreover, we provided an upperbound on the difference between the active power flow on a line under the AC and DC flow models.

Upon failures, numerical results for the single line failure analysis show that the DC power flow model provides a similar flow redistribution after single line failures as the AC flow model. On the other hand, the cascading failures simulation demonstrates that even slight errors in individual line flows can turn out to be important at cascade stages, and the metrics that capture the operational and topological aspects of the cascade can differ significantly under the two models. These results suggest that special care should be taken when drawing conclusions based on the DC cascade model in power grids. Overall, the DC cascade model can provide an overly optimistic estimation compared to the AC cascade model.

ACKNOWLEDGEMENT

This work was supported in part by Alliander N.V., DARPA RADICS under contract #FA-8750-16-C-0054, funding from the U.S. DOE OE as part of the DOE Grid Modernization Initiative, and DTRA grant HDTRA1-13-1-0021. The work of G.Z. was also supported in part by the Blavatnik ICRC.

REFERENCES

[1] J. J. Grainger and W. D. Stevenson, *Power system analysis*. McGraw-Hill, 1994.

[2] R. Baldick, B. Chowdhury, I. Dobson, Z. Dong, B. Gou, D. Hawkins, H. Huang, M. Joung, D. Kirschen, F. Li *et al.*, "Initial review of methods for cascading failure analysis in electric power transmission systems IEEE PES CAMS task force on understanding, prediction, mitigation and restoration of cascading failures," in *Proc. IEEE PES-GM'08*, July 2008.

[3] "Report on blackout in Turkey on 31st March 2015," ENTSO-E, Tech. Rep., 2015. [Online]. Available: http:/www.entsoe.eu/

[4] A. Bakshi, A. Velayutham, S. Srivastava, K. Agrawal, R. Nayak, S. Soonee, and B. Singh, "Report of the enquiry committee on grid disturbance in Northern Region on 30th july 2012 and in Northern, Eastern & North-Eastern Region on 31st July 2012," *New Delhi, India*, 2012.

[5] "Final report on the August 14th blackout in the United States and Canada: Causes and recommendations," U.S.- Canada Power System Outage Task Force, Tech. Rep., April 2004.

[6] F. Alvarado and S. Oren, "Transmission system operation and interconnection," *National transmission grid study–Issue papers*, pp. A1–A35, 2002.

[7] D. Bienstock, *Electrical Transmission System Cascades and Vulnerability: An Operations Research Viewpoint*. SIAM, 2016, vol. 22.

[8] S. Soltan, A. Loh, and G. Zussman, "Analyzing and quantifying the effect of k-line failures in power grids," *to appear in IEEE Trans. Control Netw. Syst.*, 2017.

[9] P. Crucitti, V. Latora, and M. Marchiori, "A topological analysis of the Italian electric power grid," *Physica A: Statistical Mechanics and its Applications*, vol. 338, no. 1, pp. 92–97, 2004.

[10] Y. Koç, T. Verma, N. A. Araujo, and M. Warnier, "Matcasc: A tool to analyse cascading line outages in power grids," in *Proc. IEEE IWIES'13*, 2013.

[11] S. Soltan, D. Mazauric, and G. Zussman, "Analysis of failures in power grids," *in IEEE Trans. Control Netw. Syst.*, vol. 4, no. 3, pp. 288–300, 2017.

[12] K. Purchala, L. Meeus, D. Van Dommelen, and R. Belmans, "Usefulness of DC power flow for active power flow analysis," in *IEEE PES-GM'05*, June 2005.

[13] D. Van Hertem, J. Verboomen, K. Purchala, R. Belmans, and W. Kling, "Usefulness of DC power flow for active power flow analysis with flow controlling devices," in *Proc. IET ACDC'06*, 2006, pp. 58–62.

[14] I. Dobson, *Encyclopedia of Systems and Control*, ser. Cascading network failure in power grid blackouts. Springer, 2015.

[15] B. Schäfer, D. Witthaut, M. Timme, and V. Latora, "Dynamically induced cascading failures in supply networks," *arXiv preprint arXiv:1707.08018*, 2017.

[16] P. Hines, K. Balasubramaniam, and E. C. Sanchez, "Cascading failures in power grids," *IEEE Potentials*, vol. 28, no. 5, pp. 24–30, 2009.

[17] P. D. Hines and P. Rezaei, "Cascading failures in power systems," *Smart Grid Handbook*, 2016.

[18] S. V. Buldyrev, R. Parshani, G. Paul, H. E. Stanley, and S. Havlin, "Catastrophic cascade of failures in interdependent networks," *Nature*, vol. 464, no. 7291, pp. 1025–1028, 2010.

[19] H. Xiao and E. M. Yeh, "Cascading link failure in the power grid: A percolation-based analysis," in *Proc. IEEE Int. Work. on Smart Grid Commun.*, June 2011.

[20] D. P. Chassin and C. Posse, "Evaluating North American electric grid reliability using the Barabasi–Albert network model," *Physica A*, vol. 355, no. 2-4, pp. 667 – 677, 2005.

[21] B. A. Carreras, V. E. Lynch, I. Dobson, and D. E. Newman, "Critical points and transitions in an electric power transmission model for cascading failure blackouts," *Chaos*, vol. 12, no. 4, pp. 985–994, 2002.

[22] B. A. Carreras, V. E. Lynch, I. Dobson, and D. E. Newman, "Complex dynamics of blackouts in power transmission systems," *Chaos*, vol. 14, no. 3, pp. 643–652, 2004.

[23] M. Anghel, K. A. Werley, and A. E. Motter, "Stochastic model for power grid dynamics," in *Proc. HICSS'07*, Jan. 2007.

[24] Y. Koç, M. Warnier, P. Van Mieghem, R. E. Kooij, and F. M. Brazier, "The impact of the topology on cascading failures in a power grid model," *Physica A: Statistical Mechanics and its Applications*, vol. 402, pp. 169–179, 2014.

[25] A. Asztalos, S. Sreenivasan, B. K. Szymanski, and G. Korniss, "Cascading failures in spatially-embedded random networks," *PloS one*, vol. 9, no. 1, p. e84563, 2014.

[26] J. Chen, J. S. Thorp, and I. Dobson, "Cascading dynamics and mitigation assessment in power system disturbances via a hidden failure model," *Int. J. Elec. Power and Ener. Sys.*, vol. 27, no. 4, pp. 318 – 326, 2005.

[27] A. Moussawi, N. Derzsy, X. Lin, B. K. Szymanski, and G. Korniss, "Limits of predictability of cascading overload failures in spatially-embedded networks with distributed flows," *arXiv preprint arXiv:1706.04579*, 2017.

[28] A. Bernstein, D. Bienstock, D. Hay, M. Uzunoglu, and G. Zussman, "Power grid vulnerability to geographically correlated failures - analysis and control implications," in *Proc. IEEE INFOCOM'14*, Apr. 2014.

[29] D. Bienstock, "Optimal control of cascading power grid failures," *Proc. IEEE CDC-ECC*, Dec. 2011.

[30] R. Pfitzner, K. Turitsyn, and M. Chertkov, "Controlled tripping of overheated lines mitigates power outages," *ArXiv preprint*, no. 1104.4558, Oct. 2011.

[31] P. D. Hines, I. Dobson, E. Cotilla-Sanchez, and M. Eppstein, ""dual graph" and "random chemistry" methods for cascading failure analysis," in *Proc. IEEE HICSS'13*, 2013.

[32] D. P. Nedic, I. Dobson, D. S. Kirschen, B. A. Carreras, and V. E. Lynch, "Criticality in a cascading failure blackout model," *Int. J. Elec. Power*, vol. 28, no. 9, pp. 627–633, 2006.

[33] M. Papic, K. Bell, Y. Chen, I. Dobson, L. Fonte, E. Haq, P. Hines, D. Kirschen, X. Luo, S. Miller *et al.*, "Survey of tools for risk assessment of cascading outages," in *IEEE PES-GM'11*, 2011.

[34] "Cascading failures simulator in power grids," October 2017. [Online]. Available: https://github.com/TUDelftNAS/AC-Cascade-Sim

[35] R. D. Zimmerman, C. E. Murillo-Sánchez, and R. J. Thomas, "Matpower: Steady-state operations, planning, and analysis tools for power systems research and education," *IEEE Trans. Power Syst.*, vol. 26, no. 1, pp. 12–19, 2011.

[36] R. Kaye and F. Wu, "Analysis of linearized decoupled power flow approximations for steady-state security assessment," *IEEE Trans. Circuits and Sys.*, vol. 31, no. 7, pp. 623–636, 1984.

[37] T. J. Overbye, X. Cheng, and Y. Sun, "A comparison of the AC and DC power flow models for LMP calculations," in *Proc. IEEE HICSS'04*, 2004.
[38] P. Yan and A. Sekar, "Study of linear models in steady state load flow analysis of power systems," in *IEEE PES-WM'02*, Jan. 2002.
[39] B. Stott, J. Jardim, and O. Alsaç, "DC power flow revisited," *IEEE Trans. Power Syst.*, vol. 24, no. 3, pp. 1290–1300, 2009.
[40] S. Deckmann, A. Pizzolante, A. Monticelli, B. Stott, and O. Alsac, "Numerical testing of power system load flow equivalents," *IEEE Trans. Power App. and Sys.*, no. 6, pp. 2292–2300, 1980.
[41] "Power systems test case archive," available at: http://www.ee.washington.edu/research/pstca/.
[42] J. D. Glover, M. S. Sarma, and T. Overbye, *Power System Analysis & Design, SI Version*. Cengage Learning, 2012.
[43] H. Cetinay, F. A. Kuipers, and P. Van Mieghem, "A topological investigation of power flow," *to appear in IEEE Systems Journal*, 2017.
[44] A. J. Wood and B. F. Wollenberg, *Power generation, operation, and control*, 3rd ed. John Wiley & Sons, 2012.
[45] N. Biggs, *Algebraic graph theory*. Cambridge university press, 1993.

Hale Cetinay is pursuing her Ph.D. degree since September 2014 at Delft University of Technology, The Netherlands. She obtained her M.Sc. degree (May, 2014) in Electrical and Electronics Engineering at Middle East Technical University, Turkey, where she also received her B.Sc. degree (June, 2011). Her main research interests include network science, electrical networks, and smart grids.

Saleh Soltan is a postdoctoral research associate in the department of Electrical Engineering at Princeton University. In 2017, he obtained the Ph.D. degree in Electrical Engineering from Columbia University. He received B.S. degrees in Electrical Engineering and Mathematics (double major) from Sharif University of Technology, Iran in 2011 and the M.S. degree in Electrical Engineering from Columbia University in 2012. He is the Gold Medalist of the 23rd National Mathematics Olympiad in Iran in 2005 and the recipient of Columbia University Electrical Engineering Armstrong Memorial Award in 2012.

Fernando A. Kuipers is an associate professor working on Internet Science at Delft University of Technology (TU Delft). In 2004, he obtained his Ph.D. degree cum laude; the highest possible distinction at TU Delft. His research focus is on network optimization, network resilience, Quality of Service, and Quality of Experience and addresses problems in software-defined networking, optical networking, content distribution, and cyber-physical systems/infrastructures. His work on these subjects include distinguished papers at IEEE INFOCOM 2003, Chinacom 2006, IFIP Networking 2008, IEEE FMN 2008, IEEE ISM 2008, ITC 2009, IEEE JISIC 2014, and NetGames 2015. Fernando Kuipers is senior member of the IEEE, was a visiting scholar at Technion - Israel Institute of Technology (in 2009) and Columbia University in the City of New York (in 2016), and is board member of the IEEE Benelux chapter on communications and vehicular technology and of the Royal Netherlands Society of Engineers (KIVI), section Telecommunication.

Gil Zussman received the Ph.D. degree in electrical engineering from the Technion in 2004 and was a postdoctoral associate at MIT in 2004-2007. He is currently an Associate Professor of Electrical Engineering at Columbia University. He is a co-recipient of 7 paper awards including the ACM SIGMETRICS06 Best Paper Award, the 2011 IEEE Communications Society Award for Advances in Communication, and the ACM CoNEXT'16 Best Paper Award. He received the Fulbright Fellowship, the DTRA Young Investigator Award, and the NSF CAREER Award, and was a member of a team that won first place in the 2009 Vodafone Foundation Wireless Innovation Project competition.

Piet Van Mieghem received the Masters (*magna cum laude*, 1987) and PhD (*summa cum laude*, 1991) degrees in electrical engineering from the K.U. Leuven, Leuven, Belgium. He is a Professor at the Delft University of Technology and Chairman of the section Network Architectures and Services (NAS) since 1998. His main research interests lie in modeling and analysis of complex networks and in new Internet-like architectures and algorithms for future communications networks. Before joining Delft, he worked at the Interuniversity Micro Electronic Center (IMEC) from 1987 to 1991. During 1993-1998, he was a member of the Alcatel Corporate Research Center in Antwerp, Belgium. He was a visiting scientist at MIT (1992-1993), a visiting professor at UCLA (2005), a visiting professor at Cornell University (2009), and at Stanford University (2015). He is the author of four books: Performance Analysis of Communications Networks and Systems (Cambridge Univ. Press, 2006), Data Communications Networking (Techne, 2011), Graph Spectra for Complex Networks (Cambridge Univ. Press, 2011), and Performance Analysis of Complex Networks and Systems (Cambridge Univ. Press, 2014).

APPENDIX
THE DC POWER FLOWS ACCURACY

As mentioned in Section 3.2, the DC power flow model provides a good approximation of the AC power flow model under three conditions. Here, we provide analytical insights on the accuracy of the DC power flow model.

In the following lemma, we provide an upper bound on the difference between the AC active power flows $P_{ij}^{(\text{AC})}$ and the DC active power flows $P_{ij}^{(\text{DC})}$ under those conditions.

Lemma 1. Assume the three conditions for validity of the DC power flow as a linear approximation for the AC power flow hold within following bounds:

1) $|\theta_i - \theta_j| \leq \epsilon_\theta, \forall\{i,j\} \in \mathcal{L}$,
2) $|g_{ij}/b_{ij}| \leq \epsilon_g, \forall\{i,j\} \in \mathcal{L}$,
3) $||V_i| - 1| \leq \epsilon_v, \forall i \in \mathcal{N}$,

for $\epsilon_\theta, \epsilon_v, \epsilon_g < 1$. Then, for any $1 \leq i,j \leq n$:

$$|P_{ij}^{(\text{AC})} - P_{ij}^{(\text{DC})}| \leq \epsilon \|\mathbf{B}\|_1 + \|\mathbf{P} - \tilde{\mathbf{P}}\|_1, \tag{9}$$

in which $\epsilon := 2\epsilon_g + 4\epsilon_v\epsilon_g + 2\epsilon_v^2\epsilon_g + 2\epsilon_v\epsilon_\theta + \epsilon_v^2\epsilon_\theta + \epsilon_\theta^3$ and $\|\mathbf{B}\|_1 := \sum_{i=1}^n \sum_{j=1}^n |b_{ij}|$.

Proof: Using the definition of the apparent power $S_{ik} = P_{ik}^{(\text{AC})} + \mathbf{i}Q_{ik}^{(\text{AC})}$ in (1), we have:

$$\begin{aligned} P_{ij}^{(\text{AC})} &= \Re\{V_i((V_i - V_j)(g_{ij} + \mathbf{i}b_{ij}))^*\} \\ &= \Re\{(|V_i|^2 - |V_i||V_j|e^{\mathbf{i}(\theta_i - \theta_j)})(g_{ij} - \mathbf{i}b_{ij})\} \\ &= |V_i|^2 g_{ij} - |V_i||V_j|g_{ij}\cos(\theta_i - \theta_j) \\ &\quad - |V_i||V_j|b_{ij}\sin(\theta_i - \theta_j). \end{aligned}$$

Define $\theta_i - \theta_j := \alpha_{ij}$ and $|V_i| := 1 + \beta_i$. Then:

$$\begin{aligned} ||V_i|^2 g_{ij}| &= |g_{ij} + (2\beta_i + \beta_i^2)g_{ij}| \\ &\leq |b_{ij}|(\epsilon_g + 2\epsilon_v\epsilon_g + \epsilon_v^2\epsilon_g). \end{aligned}$$

Moreover, using $|\cos(x)| \leq 1$:

$$\begin{aligned} ||V_i||V_j|g_{ij}\cos(\alpha_{ij})| &\leq |g_{ij} + (\beta_i + \beta_j + \beta_i\beta_j)g_{ij}| \\ &\leq |b_{ij}|(\epsilon_g + 2\epsilon_v\epsilon_g + \epsilon_v^2\epsilon_g). \end{aligned}$$

Using $\sin(x) = x + F(x)$, for $F(x) := -x^3/6 + O(x^5)$, we also have:

$$\begin{aligned} &- |V_i||V_j|b_{ij}\sin(\theta_i - \theta_j) = \\ &= -b_{ij}(\theta_i - \theta_j) \\ &\quad - b_{ij}\big((\beta_i + \beta_j + \beta_i\beta_j)(\theta_i - \theta_j) + F((\theta_i - \theta_j)^3)|V_i||V_j|\big), \end{aligned}$$

in which:

$$\begin{aligned} &| - b_{ij}\big((\beta_i + \beta_j + \beta_i\beta_j)(\theta_i - \theta_j) + F((\theta_i - \theta_j)^3)|V_i||V_j|\big)| \leq \\ &\leq |b_{ij}|\big(2\epsilon_v\epsilon_\theta + \epsilon_v^2\epsilon_\theta + \epsilon_\theta^3/6 + \epsilon_\theta^3\epsilon_v/3 + \epsilon_\theta^3\epsilon_v^2/6\big) \\ &\leq |b_{ij}|\big(2\epsilon_v\epsilon_\theta + \epsilon_v^2\epsilon_\theta + \epsilon_\theta^3\big). \end{aligned}$$

Hence,

$$P_{ij}^{(\text{AC})} = -b_{ij}(\theta_i - \theta_j) + e_{ij}, \tag{10}$$

in which:

$$|e_{ij}| \leq |b_{ij}|\big(2\epsilon_g + 4\epsilon_v\epsilon_g + 2\epsilon_v^2\epsilon_g + 2\epsilon_v\epsilon_\theta + \epsilon_v^2\epsilon_\theta + \epsilon_\theta^3\big).$$

Notice that $-b_{ij}(\theta_i - \theta_j)$ is not necessarily equal to $P_{ij}^{(\text{DC})} = -b_{ij}(\tilde{\theta}_i - \tilde{\theta}_j)$ since θ_i and θ_j are obtained from the AC power flow model, which are different from the phase angles obtained by the DC power flow model. However, we can compute the difference between these two values by writing the power flow equations using (10) as follows:

$$\begin{aligned} \text{AC:} &- \mathbf{B\Theta} + \mathbf{E} = \mathbf{P} \\ &- \mathbf{B\Theta} = \tilde{\mathbf{P}} - \mathbf{E} + (\mathbf{P} - \tilde{\mathbf{P}}) \\ \text{DC:} &- \mathbf{B}\tilde{\mathbf{\Theta}} = \tilde{\mathbf{P}} \end{aligned}$$

in which $\mathbf{E}$ is an $n \times 1$ vector with the i^{th} entry equal to e_i such that $|e_i| \leq \sum_{j \in N(i)} |e_{ij}|$. Recall that vectors $\mathbf{P}$ and $\tilde{\mathbf{P}}$ are equal except (depending on the lossless assumption) in the *slack bus* (first entry). From the flow equations and the superpositions principle, the difference between $-b_{ij}(\theta_i - \theta_j)$ and $-b_{ij}(\tilde{\theta}_i - \tilde{\theta}_j)$ cannot be greater than the maximum flow that vector $\mathbf{E} - (\mathbf{P} - \tilde{\mathbf{P}})$ can produce which is at most $\|\mathbf{P} - \tilde{\mathbf{P}}\|_\mathbf{1} + (\sum_{i=1}^n \sum_{j \in N(i)} |b_{ij}|)(2\epsilon_g + 4\epsilon_v\epsilon_g + 2\epsilon_v^2\epsilon_g + 2\epsilon_v\epsilon_\theta + \epsilon_v^2\epsilon_\theta + \epsilon_\theta^3)$. Hence, a conservative bound for the difference between the AC and DC active power flows is:

$$|P_{ij}^{(\text{AC})} - P_{ij}^{(\text{DC})}| \leq \epsilon \|\mathbf{B}\|_1 + \|\mathbf{P} - \tilde{\mathbf{P}}\|_1.$$

□

The following corollaries, which immediately follow from Lemma 1, demonstrate the bounds for the difference between the AC and DC active power flows for the special cases of a lossless network (i.e., $\epsilon_g = 0$).

Corollary 1. If the lines are lossless ($\epsilon_g = 0$), then for any $1 \leq i,j \leq n$:

$$|P_{ij}^{(\text{AC})} - P_{ij}^{(\text{DC})}| \leq (2\epsilon_v\epsilon_\theta + \epsilon_v^2\epsilon_\theta + \epsilon_\theta^3)\|\mathbf{B}\|_1.$$

Corollary 2. If the lines are lossless ($\epsilon_g = 0$), and for all the lines $b_{ij} = -1$, then for any $1 \leq i,j \leq n$:

$$|P_{ij}^{(\text{AC})} - P_{ij}^{(\text{DC})}| \leq 4(2\epsilon_v\epsilon_\theta + \epsilon_v^2\epsilon_\theta + \epsilon_\theta^3)|\mathcal{L}|.$$

In the following proposition, we demonstrate that if the power network topology is a tree, we can improve the bound in Corollary 1 and prove that the DC power flows are equal to the AC active power flows.

Proposition 1. If $\mathcal{G}$ is a tree and $\epsilon_g = 0$, then $\forall 1 \leq i,j \leq n$: $P_{ij}^{(\text{AC})} = P_{ij}^{(\text{DC})}$.

Proof: We want to show that $P_{ij}^{(\text{DC})} = P_{ij}^{(\text{AC})}, \forall\{i,j\} \in \mathcal{L}$ is a DC power flow solution for this instance. As all the lines are purely reactive, the network is lossless and in the AC power flows $|P_{ij}^{(AC)}| = |P_{ji}^{(AC)}|, \forall\{i,j\} \in \mathcal{L}$. From Kirchhoff's laws, we also have $\sum_{j \in N(i)} P_{ij}^{(\text{AC})} = P_i$. Hence, setting $P_{ij}^{(\text{DC})} = P_{ij}^{(\text{AC})}$ completely satisfies the active power flow conservation in equation (4). It remains to prove that there are phase angles satisfying equation (4) with $P_{ij}^{(\text{DC})} = P_{ij}^{(\text{AC})}$. Since $\mathcal{G}$ is a tree, $m = n - 1$. Hence, $P_{ij}^{(\text{DC})} = -b_{ij}(\tilde{\theta}_i - \tilde{\theta}_j)$ for all $\{i,j\} \in \mathcal{L}$ consists of $n-1$ independent linear equations for n variables $\tilde{\theta}_1, \tilde{\theta}_2, \ldots, \tilde{\theta}_n$ (It is known that for a connected graph G, $\text{rank}(\mathbf{B}) = n - 1$ [45]). As a result, by choosing $\tilde{\theta}_1 = 0$, all other phase angles can be found uniquely. Hence, $P_{ij}^{(\text{DC})} = P_{ij}^{(\text{AC})}$ is the DC power flow solution for this instance as well.

□